

Higher-order schemes for 3D first-arrival traveltimes and amplitudes

Songting Luo¹, Jianliang Qian¹, and Hongkai Zhao²

ABSTRACT

In the geometrical-optics approximation for the Helmholtz equation with a point source, traveltimes and amplitudes have upwind singularities at the point source. Hence, both first-order and higher-order finite-difference solvers exhibit formally at most first-order convergence and relatively large errors. Such singularities can be factored out by factorizing traveltimes and amplitudes, where one factor is specified to capture the corresponding source singularity and the other factor is an unknown function smooth near the source. The resulting underlying unknown functions satisfy factored eikonal and transport equations, respectively. A third-order Lax-Friedrichs scheme is designed to compute the underlying functions. Thus, highly accurate first-arrival traveltimes and reliable amplitudes can be computed. Furthermore, asymptotic wavefields are constructed using computed traveltimes and amplitudes in the WKBJ form. Two-dimensional and 3D examples demonstrate the performance of the proposed algorithms, and the constructed WKBJ Green's functions are in good agreement with direct solutions of the Helmholtz equation before caustics occur.

INTRODUCTION

The point-source Green's function for the Helmholtz equation is fundamental for seismic modeling, migration, and inversion. However, it is very costly and difficult to solve the Helmholtz equation directly when the frequency-related wavenumber parameter is large; consequently, some approximate methods such as one-way wave equations and geometrical optics are used frequently. In geometrical optics approximations for high-frequency wave propagation, the point-source traveltime has an upwind source singularity, which makes it extremely difficult to numerically compute the traveltime

field with high accuracy even by higher-order finite-difference eikonal solvers. The resultant inaccurate traveltimes prevent reliable computations of takeoff angles, out-of-plane curvatures, and amplitudes. Even with accurate traveltime fields, the source singularity of takeoff angles, out-of-plane curvatures, and amplitudes can also make it difficult to obtain high accuracy with usual finite-difference schemes.

Many finite-difference schemes have been introduced to solve the eikonal equation with point-source conditions for first-arrival traveltimes (Vidale, 1990; van Trier and Symes, 1991; Qin et al., 1992; Schneider et al., 1992; Schneider, 1995; Kim and Cook, 1999; Sethian and Popovici, 1999; Qian and Symes, 2002a, 2002b; Tsai et al., 2003; Kao et al., 2004; Zhao, 2005; Leung and Qian, 2006; Qian et al., 2007a, 2007b, Benamou et al., 2010).

Most of these finite-difference schemes suffer from the upwind source singularity; in some situations, if the point-source traveltime is not initialized properly, the so-called traveltime reciprocity discrepancy can appear as shown in Tryggvason and Bergman (2006) for the eikonal solver *time3d* developed in Podvin and Lecomte (1991). Special treatments such as initializing the traveltime field in a fixed grid-independent region of constant velocity near the source point are employed to obtain high accuracy (Zhang et al., 2006; Benamou et al., 2010; Serna and Qian, 2010). These methods have drawbacks such as: (1) the velocity may not be homogeneous near the source, and/or (2) the size of the region of analytic computations must be set by the user and bears no direct relation to the grid parameters. The drawbacks of these methods can be overcome with the adaptive grid-refinement method as proposed in Qian and Symes (2002a). However, the adaptive grid-refinement method requires some subtle data structures in numerical implementation.

In Luo and Qian (2011), these difficulties in computing higher-order accurate first-arrival traveltimes and amplitudes are overcome with a factorization approach. The idea of factorization with respect to constant velocity solutions has been used as celerity parameterization in Pica (1997) and Zhang et al. (2005), and it was further developed in Fomel et al. (2009) to treat point-source singularity in the context of first-order fast sweeping methods for eikonal equations. Inspired by the factored eikonal equation in Fomel

Manuscript received by the Editor 9 November 2010; revised manuscript received 30 August 2011; published online 24 February 2012.

¹Michigan State University, Department of Mathematics, East Lansing, Michigan, USA. E-mail: luos@math.msu.edu; qian@math.msu.edu.

²University of California, Department of Mathematics, Irvine, California, USA. Email: zhao@math.uci.edu.

© 2012 Society of Exploration Geophysicists. All rights reserved.

et al. (2009), Luo and Qian (2011) first proposed to factor the take-off angle additively and the out-of-plane curvature multiplicatively so that the source singularities are well-captured by known functions corresponding to constant velocities; then based on these factorizations, they further designed a weighted essentially non-oscillatory (WENO) (Liu et al., 1994; Jiang and Shu, 1996; Jiang and Peng, 2000) based Lax-Friedrichs scheme to compute the resulting underlying functions which are smooth near the source point; thus, they were able to compute the traveltime, the takeoff angle, and the amplitude with high accuracy.

In this work, we apply this factorization approach directly to the amplitude without calculating the takeoff angle and the out-of-plane curvature. We factor the amplitude into two multiplicative factors, one of which is the amplitude for a homogeneous medium. This factor captures the source singularity so that the other factor (the underlying function) is smooth near the source. Then we apply the third-order WENO-based Lax-Friedrichs sweeping scheme (Kao et al., 2004; Zhang et al., 2006; Luo and Qian, 2011) to numerically compute the underlying function. Therefore, we are able to compute the amplitude accurately in both 2D and 3D cases.

All the above cited works and discussions hinge on the concept of viscosity solution (Crandall and Lions, 1983) which singles out a unique, globally defined, physically relevant weak solution among many possible generalized solutions for the eikonal equation, and the resulting solution is the so-called first-arrival traveltime. Although the usefulness of first-arrival traveltimes for Kirchhoff migration has been questioned in Geoltrain and Brac (1993) and Gray and May (1994) because the first-arrival traveltimes in complex media usually do not correspond to the most energetic traveltimes crucial for imaging complex structures (Nichols, 1994), the first-arrival based Kirchhoff migration methods can still be used as long as velocity variations do not generate multiple arrivals as illustrated in Gray and May (1994). On the other hand, Bevc (1997) has used first-arrival traveltimes in his semi-recursive Kirchhoff migration to image the Marmousi model successfully by partitioning the imaging domain into several subdomains and carrying out recursive wave-equation datuming and Kirchhoff migration in a layer-stripping fashion. Moreover, first-arrival eikonal solvers are essential components for developing efficient algorithms for computing multiple arrivals in a domain-decomposition-type manner (Symes and Qian, 2003; Rawlinson and Sambridge, 2004), though a popular trend for computing multiple arrivals is to use a phase-space formulation as shown in the following references: Engquist et al. (2002); Fomel and Sethian (2002); Osher et al. (2002); Qian et al. (2003); Leung et al. (2004, 2007); Qian and Leung (2004, 2006).

We mention that higher-order accurate first-arrival traveltimes are also important in solving linearized eikonal equations with respect to the velocity which arise in traveltime tomography (Aldridge, 1994; Franklin and Harris, 2001; Alkhalifah, 2002; Leung and Qian, 2006; Taillandier et al., 2007, 2008, 2009) and in solving linearized eikonal equations with respect to the source location which arise in velocity estimation (Alkhalifah and Fomel, 2010). In these linearized eikonal equations, the traveltime gradient appears as the coefficient, which usually is obtained by numerically differentiating computed traveltimes, thus higher-order accurate traveltimes will be crucial for solving linearized eikonal equations with high accuracy. Therefore, the higher-order schemes for first-arrival traveltimes and amplitudes proposed here will be useful in many applications, such

as semi-recursive Kirchhoff migration (Bevc, 1997), traveltime tomography (Leung and Qian, 2006; Taillandier et al., 2007, 2008, 2009), and velocity estimation (Alkhalifah and Fomel, 2010).

In terms of computing traveltimes, one can use ray-tracing methods and their variants (Cerveny et al., 1977; Vinje et al., 1993, 1996; Meng and Bleistein, 1997; Sava and Fomel, 2001) which yield not only first arrivals but also multiple arrivals. However, ray-tracing based methods suffer from nonuniform distribution of rays with inevitable shadow zones and cumbersome interpolation onto uniform meshes. To obtain traveltimes distributed on uniform meshes, one can also utilize the shooting method to solve two-point boundary value problems for every source-receiver pair (Pereyra et al., 1980). However, such shooting methods might fail to converge in complex velocity media and might not yield first-arrival traveltimes. Moreover, the shooting method is difficult to implement in 3D cases. On the other hand, the first-order version of the proposed method is proved to be convergent and unconditionally stable (Serna and Qian, 2010), and it is guaranteed to yield first-arrival traveltimes on uniform meshes; in addition, the proposed higher-order schemes are easy to implement in 2D and 3D cases.

A natural question is: what are the advantages that the proposed higher-order schemes for first-arrival traveltimes and amplitudes bring to bear? The advantages are multifold. First, to achieve a certain specified accuracy, a higher-order scheme needs a much coarser mesh than a first-order scheme does, thus higher-order schemes are much more efficient than first-order schemes in terms of computational cost. Second, higher-order accurate traveltimes can be numerically differentiated to yield reliable traveltime gradients while first-order accurate traveltimes cannot, as demonstrated in Qian and Symes (2002a). Consequently, our proposed higher-order schemes for traveltimes will be significant for solving linearized eikonal equations in traveltime tomography (Leung and Qian, 2006; Taillandier et al., 2009) and velocity estimation (Alkhalifah and Fomel, 2010). Third, because according to geometrical-optics, traveltime and amplitude functions are independent of the frequency parameter in the Helmholtz equation, traveltimes and amplitudes computed by the proposed higher-order schemes on a fixed uniform mesh can be used to construct Green's functions for the Helmholtz equation for all the frequencies in a certain frequency band as long as no aliasing appears. At this point, we recall that the frequency parameter in the Helmholtz equation needs to be fixed at the start when one solves the equation directly to compute the Green's function. Therefore, the proposed higher-order schemes for traveltimes and amplitudes will be useful for constructing Green's functions for multiple frequencies, which are exactly needed for Kirchhoff migration and imaging.

This paper is organized as follows. We begin presenting the methodology by first recalling the factorization for the traveltime in Fomel et al. (2009) and Luo and Qian (2011), then we present the factorization for the amplitude. We further present the third-order WENO-based Lax-Friedrichs scheme to solve the factored equations in 3D (Kao et al., 2004; Zhang et al., 2006; Luo and Qian, 2011). Both 2D and 3D examples are presented in numerical experiments. We use our results to construct asymptotic Green's functions and compare the resulting Green's functions with those obtained by the Helmholtz solver in Erlangga et al. (2006) and Engquist and Ying (2011). Concluding remarks are given at the end.

METHODOLOGY

Traveltime and amplitude

For a source (x_0, y_0, z_0) in an isotropic solid, the traveltime $\tau(x, y, z)$ is the viscosity solution of an eikonal equation (Lions, 1982; Crandall and Lions, 1983),

$$|\nabla\tau| = s(x, y, z), \tag{1}$$

with the initial condition

$$\lim_{(x,y,z) \rightarrow (x_0,y_0,z_0)} \left(\frac{\tau(x,y,z)}{\sqrt{(x-x_0)^2 + (y-y_0)^2 + (z-z_0)^2}} - \frac{1}{v(x,y,z)} \right) = 0, \tag{2}$$

where $v = 1/s$ is the velocity.

Based on the traveltime field, one can approximate the amplitude field by solving a transport equation (Cerveny et al., 1977),

$$\nabla\tau \cdot \nabla A + \frac{1}{2} A \nabla^2 \tau = 0. \tag{3}$$

Equation 3 is a first-order advection equation for the amplitude A . To get a first-order accurate amplitude field, one needs a third-order accurate traveltime field because the Laplacian of the traveltime field is involved (Qian and Symes, 2002a).

Traveltime τ and amplitude A have an upwind singularity at the source (x_0, y_0, z_0) . Any first-order or higher-order finite-difference eikonal solvers or finite-difference methods for the amplitude formally can have at most first-order convergence and large errors because the low accuracy near the source can spread out to the whole space. In Qian and Symes (2002a), an adaptive method based on the WENO technique for the paraxial eikonal equation overcomes this difficulty. The mesh needs to be refined near the source until expected accuracy requirement is satisfied. In Fomel et al. (2009), the traveltime is factorized into two multiplicative factors, one of which is already known and captures the source singularity. This factorization results in an underlying function that is smooth near the source. The underlying function satisfies a factored eikonal equation. Numerical schemes can be designed to compute the underlying function. As a consequence, the accuracy of the traveltime can be greatly improved as demonstrated in Fomel et al. (2009). This factorization approach has been extended in Luo and Qian (2011) for takeoff angles and out-of-plane curvatures to obtain reliable amplitudes. Takeoff angles can be decomposed into two additive factors and out-of-plane curvatures can be decomposed into two multiplicative factors. In both cases, one of the two factors is known corresponding to a homogeneous medium and captures the source singularity.

In this work, we apply the factorization idea to the amplitude A in the transport equation 3. We decompose A into two multiplicative factors. One of them is the amplitude corresponding to a constant velocity field, and it is known analytically. The factorization of A results in an underlying function that satisfies a factored advection equation. For the factored equations, we use the Lax-Friedrichs scheme based on third-order WENO differences (Kao et al., 2004; Zhang et al., 2006; Luo and Qian, 2011) to solve them numerically.

Factorization of traveltime and amplitude

Consider the following factored decompositions (Fomel et al., 2009; Luo and Qian, 2011),

$$\begin{cases} \tau(x, y, z) = \tau_0(x, y, z)u(x, y, z), \\ s(x, y, z) = s_0(x, y, z)\alpha(x, y, z), \end{cases} \tag{4}$$

and assume that τ_0 satisfies

$$|\nabla\tau_0| = s_0, \tag{5}$$

with the initial condition,

$$\lim_{(x,y,z) \rightarrow (x_0,y_0,z_0)} \left(\frac{\tau_0(x,y,z)}{\sqrt{(x-x_0)^2 + (y-y_0)^2 + (z-z_0)^2}} - s_0(x,y,z) \right) = 0. \tag{6}$$

If we choose s_0 as some constant, we have

$$\tau_0 = \frac{\sqrt{(x-x_0)^2 + (y-y_0)^2 + (z-z_0)^2}}{v_0},$$

which is the traveltime corresponding to the constant velocity field $v_0 = 1/s_0$.

The function substitution transforms the eikonal equation 1 into the factored eikonal equation (Fomel et al., 2009; Luo and Qian, 2011),

$$\sqrt{\tau_0^2 |\nabla u|^2 + 2\tau_0 u \nabla\tau_0 \cdot \nabla u + u^2 s_0^2} = s. \tag{7}$$

The factor τ_0 captures the source singularity such that the underlying function u is smooth in a neighborhood of the source.

Denote A_0 as the amplitude corresponding to the constant velocity v_0 , and consider the following decomposition for A :

$$A(x, y, z) = A_0(x, y, z)D(x, y, z). \tag{8}$$

Substituting $A = A_0 D$ and $\tau = \tau_0 u$ into equation 3, we get the factored transport equation,

$$A_0(\tau_0 \nabla u + u \nabla\tau_0) \cdot \nabla D + \left(\tau_0 \nabla u \cdot \nabla A_0 + A_0 \nabla\tau_0 \cdot \nabla u + \frac{1}{2} A_0 \tau_0 \Delta u \right) D = 0. \tag{9}$$

A_0 is known analytically and captures the source singularity, thus the underlying factor D is smooth in a neighborhood of the source.

To get first-order accurate A , we need first-order accurate D . In the factored transport equation 9, to get first-order accurate D , we need at least third-order accurate u , because Δu is involved. Therefore, we need to solve the factored eikonal equation 7 for u with at least third-order accuracy. Traveltime τ_0 and amplitude A_0 corresponding to the constant velocity field v_0 capture the source singularity properly, which makes it easy to design high-order methods to solve equations 7 and 9 for the underlying functions u and D .

Lax-Friedrichs scheme based on third-order WENO

We present the Lax-Friedrichs scheme for the factored equations 7 and 9 on a rectangular mesh Ω^h with grid size h covering the domain Ω (Kao et al., 2004; Zhang et al., 2006; Luo and Qian, 2011). Consider the following equation in a generic form,

$$H(x, y, z, u, u_x, u_y, u_z) = f(x, y, z). \quad (10)$$

At a grid point $(i, k, j) = (x_i, y_k, z_j)$ with neighbors,

$$N\{i, k, j\} = \{(x_{i-1}, y_k, z_j), (x_{i+1}, y_k, z_j), (x_i, y_k, z_{j-1}), (x_i, y_k, z_{j+1}), (x_i, y_{k+1}, z_j), (x_i, y_{k-1}, z_j)\},$$

we design a third-order WENO-based Lax-Friedrichs scheme for this equation as detailed in Appendix A.

Consequently, the third-order Lax-Friedrichs sweeping method for equation 10 is summarized as follows (Kao et al., 2005; Zhang et al., 2006; Luo and Qian, 2011):

- 1) Initialization: assign exact values or interpolate values at grid points within a cubic volume centered at the source point with side-length equal to $2h + 2h$, such that the number of grid points is enough for the third-order WENO approximations. These values are fixed during iterations.
- 2) Iterations: update $u_{i,k,j}^{\text{new}}$ in equation A-11 by Gauss-Seidel iterations with eight alternating directions

- (1) $i = 1:I, k = 1:K, j = 1:J;$
- (2) $i = 1:I, k = 1:K, j = J:1;$
- (3) $i = 1:I, k = K:1, j = 1:J;$
- (4) $i = 1:I, k = K:1, j = J:1;$
- (5) $i = I:1, k = 1:K, j = 1:J;$
- (6) $i = I:1, k = 1:K, j = J:1;$
- (7) $i = I:1, k = K:1, j = 1:J;$
- (8) $i = I:1, k = K:1, j = J:1.$

- 3) Convergence: if

$$\left| u_{i,k,j}^{\text{new}} - u_{i,k,j}^{\text{old}} \right|_{\infty} \leq \delta,$$

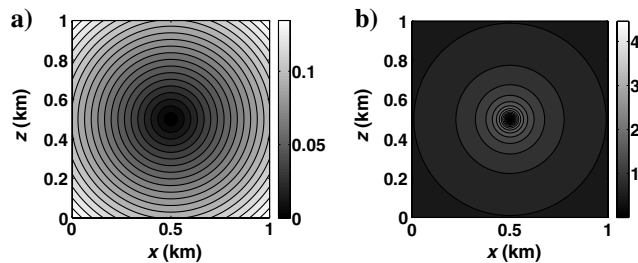


Figure 1. 2D example 1. Computed (a) traveltimes and (b) amplitudes.

where δ is a given convergence threshold value, the iteration converges and stops.

We use this scheme to solve the factored equations:

- Equation 7 with Hamiltonian H and f as,

$$H(x, y, z, u, u_x, u_y, u_z) = \sqrt{\tau_0^2 |\nabla u|^2 + 2\tau_0 u \nabla \tau_0 \cdot \nabla u + u^2 \tau_0^2},$$

$$f = s.$$

- Equation 9 with Hamiltonian H and f as,

$$H(x, y, z, D, D_x, D_y, D_z) = A_0(\tau_0 \nabla u + u \nabla \tau_0) \cdot \nabla D$$

$$+ (\tau_0 \nabla u \cdot \nabla A_0 + A_0 \nabla \tau_0 \cdot \nabla u + \frac{1}{2} A_0 \tau_0 \Delta u) D,$$

$$f = 0.$$

NUMERICAL EXPERIMENTS

In this section, we present several 2D and 3D examples to demonstrate the performance of the method. For all the examples, the convergence criterion δ is chosen to be 10^{-9} .

2D examples

For all 2D examples, we show computed traveltimes and amplitudes, and we use computed results to approximate Green's functions for the Helmholtz equation with high frequencies,

$$\nabla^2 G_2(x, z, \omega) + \frac{\omega^2}{v^2(x, z)} G_2(x, z, \omega)$$

$$= -\delta(x - x_0) \delta(z - z_0), \quad (11)$$

where $G_2(x, z, \omega)$ is the Green's function dependent on the frequency ω .

We approximate the 2D Green's function in the WKBJ form (See Page 38 in Babich and Buldyrev, 2009 or Appendix C in Leung et al., 2007),

$$G_2(x, z, \omega) \approx \frac{1}{\sqrt{\omega}} A(x, z) e^{i(\omega \tau(x, z) + \frac{\pi}{4})}. \quad (12)$$

First, we use the following two velocity models, and we compare the WKBJ Green's functions with the direct solutions by a Helmholtz solver. We choose $\omega = 32\pi$.

- 1) Constant velocity $v(x, z) \equiv 5.0$ km/s, $(x_0, z_0) = (0.5, 0.5)$ km, and domain $[0, 1] \times [0, 1]$ km. We apply our method on a 100×100 mesh and solve the Helmholtz equation 11 with the Helmholtz solver (Erlangga et al., 2006) on a 1200×1200 mesh. Figure 1 shows the traveltimes and amplitude computed with our method. Figure 2 shows the results for the 2D Green's function on a 100×100 mesh. The results by our method are very close to those obtained by the Helmholtz solver. The reason is that the traveltimes field is smooth everywhere away from the source. Therefore, the constructed asymptotic Green's function approximates the true Green's function faithfully.
- 2) Velocity $v(x, z) = 1 + 0.2 \sin(0.5\pi z) \sin(3\pi(x + 0.05))$ km/s, $(x_0, z_0) = (0.5, 0.1)$ km/s, and domain $[0, 1] \times [0, 2]$ km. We apply our method on a 200×100 mesh and solve the Helmholtz equation 11 with the Helmholtz solver (Erlangga et al., 2006) on

a 1600×800 mesh. Figure 3 shows the velocity model and the resulting traveltime and amplitude computed by our method. Figure 4 shows the results for the 2D Green's function on a 200×100 mesh; especially we plot two slices at $z = 0.3$ km (no kink and no caustic) and at $z = 1.5$ km (kink and caustic). The constructed Green's function in the weak sense cannot approximate the true Green's function faithfully because the traveltime field is not smooth. However, we notice that before kinks occur in the single-valued traveltime field or caustics occur in the multivalued traveltime field, the true traveltime field is smooth and the asymptotic Green's function in the single-valued sense approximates the true Green's function faithfully. Only after kinks in the single-valued traveltime field

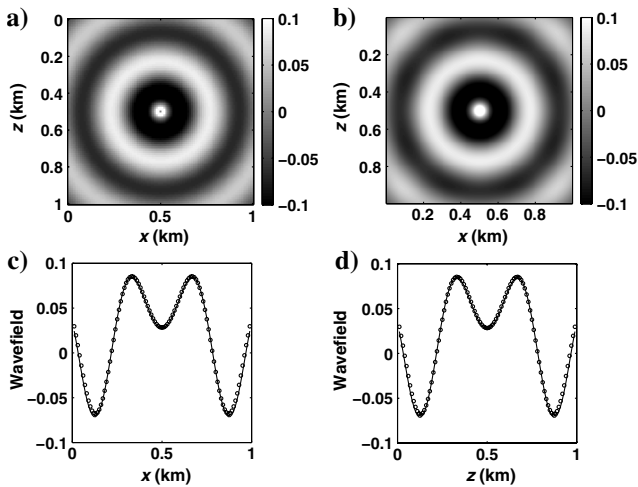


Figure 2. 2D example 1. Green's function with $\omega = 32\pi$. (a) Real part of the Green's function by our method. (b) Real part of the Green's function by Helmholtz solver. (c) Real part of the Green's function at $z = 0.3$ km. Circle is our method; line is the Helmholtz solver. (d) Real part of the Green's function at $x = 0.3$ km. Circle is our method; line is the Helmholtz solver.

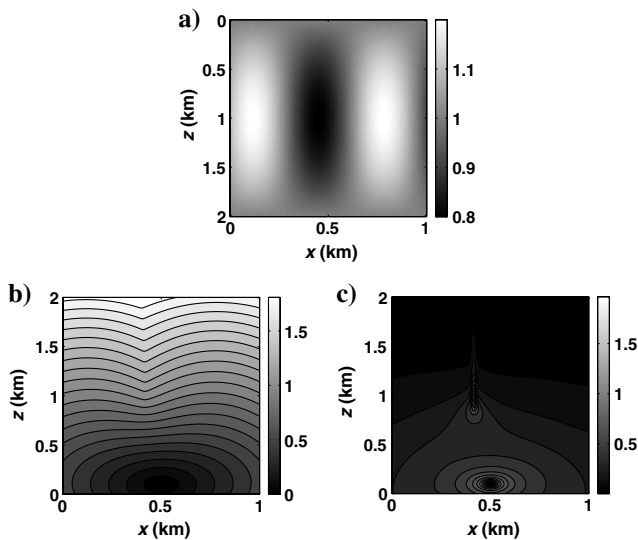


Figure 3. 2D example 2. (a) Velocity field, (b) computed traveltimes, and (c) computed amplitudes.

or caustics in the multivalued traveltime field appear, the two traveltime fields yield totally different Green's functions. Figure 5 shows the rays computed with the single-valued traveltime field by integrating the backward characteristic equation $\frac{dx}{dt} = -\nabla\tau$, and the rays computed by ray-tracing technique. Clearly, one can observe the kinks and caustics.

Marmousi velocity model

We apply our algorithms to the smooth Marmousi velocity model as in Figure 6a. The model is sampled on a 0.024 km by 0.024 km grid, consisting of 384 samples in the x -direction and 122 samples in the z -direction; therefore the domain is $[0, 9.192] \times [0, 2.904]$ km. The point source is chosen to be at $(6.0, 2.784)$ km.

Traveltimes and amplitudes by our method are shown in Figures 6b and 6c, where the two functions are computed on the original mesh of 384×122 . Figure 7 compares the first-arrival based asymptotic Green's function and the Green's function obtained by a nine-point finite-difference direct Helmholtz solver (Jo et al., 1996), where $\omega = 32\pi$. A perfectly matched layer

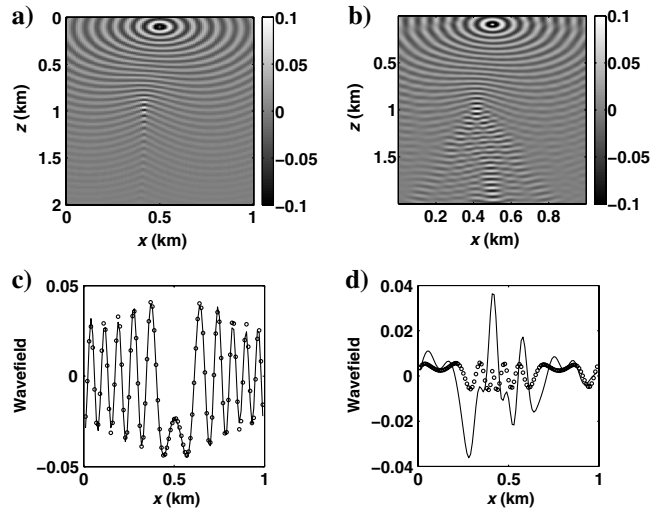


Figure 4. 2D example 2. Green's function with $\omega = 32\pi$. (a) Real part of the Green's function by our method. (b) Real part of the Green's function by Helmholtz solver. (c) Real part of the Green's function at $z = 0.3$ km with circle: our method and line: Helmholtz solver. (d) Real part of the Green's function at $z = 1.5$ km. Circle is our method; and line is the Helmholtz solver.

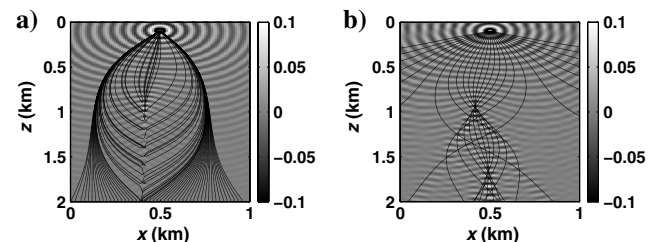


Figure 5. 2D example 2. Green's functions with computed rays. $\omega = 32\pi$. (a) Real part of the Green's function by our method, and rays computed with single-valued traveltime field. (b) Real part of the Green's function by Helmholtz solver, and rays computed by ray-tracing technique.

(PML) absorbing boundary condition (Berenger, 1994) is used in the direct solver. The first-arrival based asymptotic Green's function is constructed directly on the same mesh of 384×122 as used to compute traveltimes and amplitudes. To resolve highly oscillatory wavefields arising from complex velocity structure by the direct solver, the original Marmousi velocity model has been interpolated linearly onto a very fine mesh of 3831×1211 , and the direct Helmholtz solver is applied to the resulting refined Marmousi

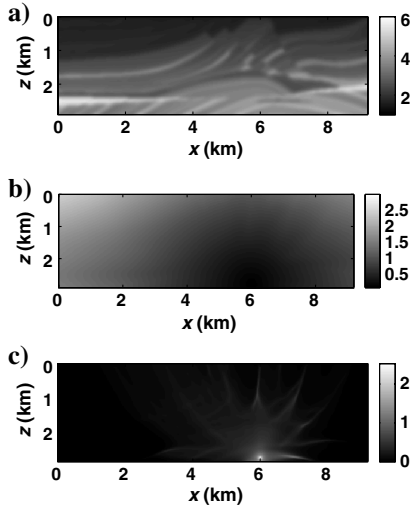


Figure 6. 2D example 3: Marmousi model. (a) Velocity field, (b) computed traveltimes, and (c) computed amplitudes.

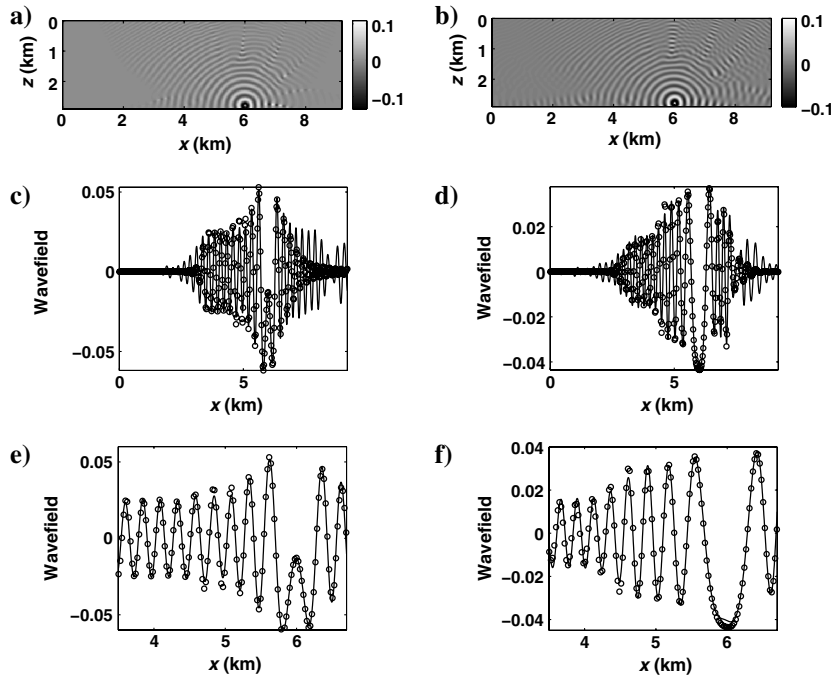


Figure 7. 2D example 3: Marmousi model. Green's function with $\omega = 32\pi$. (a) Green's function constructed by our method. (b) Green's function computed by Helmholtz solver. (c) Real part of the Green's function at $z = 2.496$ km with circle: our method and line: Helmholtz solver. (d) Real part of the Green's function at $z = 1.992$ km with circle: our method and line: Helmholtz solver; (e) part of (c) with $3.5 < x < 6.7$ km; and (f) part of (d) with $3.5 < x < 6.7$ km.

model. To see differences between the two Green's functions more clearly, we plot two slices at $z = 2.496$ km and $z = 1.992$ km in Figure 7c and 7d. Because the Marmousi model is highly heterogeneous with both lateral and in-depth variations, caustics quickly develop away from the source as shown in Figure 7a and 7b. Although the comparisons in Figure 7c and 7d show that the two Green's functions might not match with each other globally, they do match with each other locally in a neighborhood of the source as shown in Figure 7e and 7f. In the neighborhood of the source, the traveltime field is single-valued so that the first-arrival based asymptotic Green's function approximates the true Green's function faithfully.

Because traveltime and amplitude functions are independent of frequency ω , we can use a very coarse mesh to compute these two functions. As long as no aliasing occurs in the constructed Green's function, we can use the computed traveltime and amplitude functions to construct Green's functions in a broad band of frequencies. This is in sharp contrast to a direct Helmholtz solver, which is frequency dependent and might require very fine mesh arising from high frequencies as shown in the results for the Marmousi model.

3D examples

We use two 3D velocity models to demonstrate the performance of our method. With computed traveltimes and amplitudes at our disposal, we approximate 3D Green's functions for the Helmholtz equation with high frequencies,

$$\nabla^2 G_3(x, y, z, \omega) + \frac{\omega^2}{v^2(x, y, z)} G_3(x, y, z, \omega) = -\delta(x - x_0)\delta(y - y_0)\delta(z - z_0), \quad (13)$$

where $G_3(x, y, z, \omega)$ is the Green's function dependent on the frequency ω .

We approximate the 3D Green's function in the WKB form (See Page 38 in Babich and Buldyrev [2009] or Appendix C in Leung et al. [2007]),

$$G_3(x, y, z, \omega) \approx A(x, y, z)e^{i\omega\tau(x, y, z)}. \quad (14)$$

3D example 1: constant velocity. The velocity $v \equiv 5$ km/s. The domain $[-1, 1] \times [-1, 1] \times [-1, 2]$ km. We use an $81 \times 81 \times 121$ mesh. The source point is at $(x_0, y_0, z_0) = (0, 0, 0)$ km. We choose $\omega = 64\pi$. Figure 8 shows the computed traveltime, amplitude and constructed Green's functions. In Figure 9, we compare our computed amplitude with the exact amplitude

$$A(x, y, z) = \frac{1}{4\pi\sqrt{(x - x_0)^2 + (y - y_0)^2 + (z - z_0)^2}},$$

at $(y = 0, z = 0.3)$ km and $(y = 0, z = 1.5)$ km, and we also compare the constructed Green's functions with the exact asymptotic form obtained in Leung et al. (2007) at $(y = 0, z = 0.3)$ km and $(y = 0, z = 1.5)$ km. The comparison indicates that the computed amplitudes and constructed Green's functions are accurate.

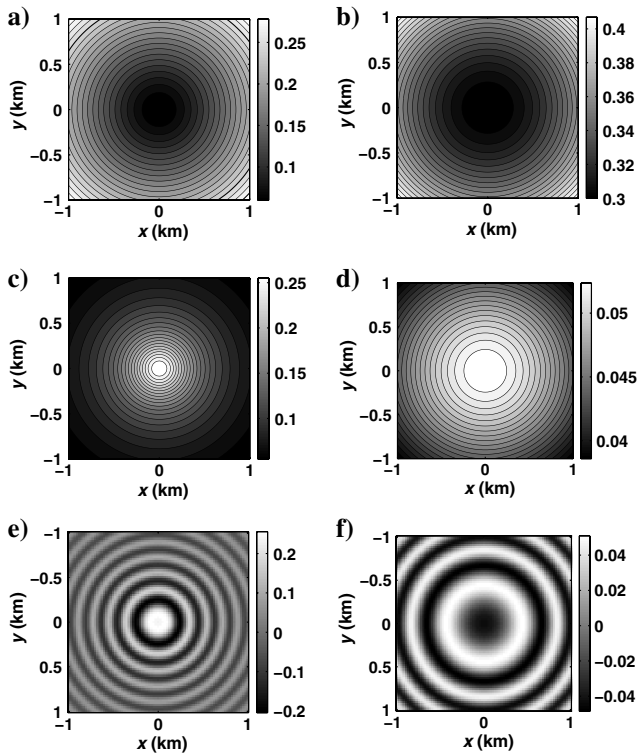


Figure 8. 3D example 1. At depth $z = 0.3$ km: (a) traveltimes, (c) amplitudes, and (e) constructed Green's function with $\omega = 64\pi$. At depth $z = 1.5$ km: (b) traveltimes, (d) amplitudes, and (f) constructed Green's function with $\omega = 64\pi$.

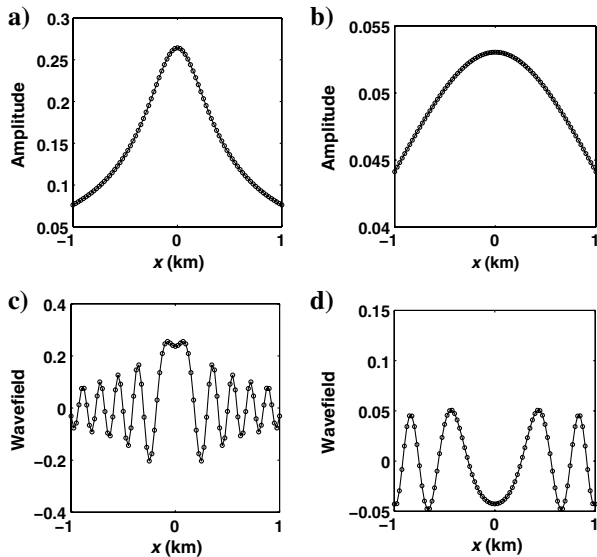


Figure 9. 3D example 1. Comparison. (a) Amplitudes at $(y = 0, z = 0.3)$ km; (b) amplitudes at $(y = 0, z = 1.5)$ km; (c) Green's functions with $\omega = 64\pi$ at $(y = 0, z = 0.3)$ km; and (d) Green's functions with $\omega = 64\pi$ at $(y = 0, z = 1.5)$ km. Circle: our method; line: exact solution.

3D example 2: Vinje's Gaussian model. The model is given on the domain is $[0, 1] \times [0, 1] \times [0, 1]$ km by,

$$v(x, y, z) = 4 - 1.75e^{-\frac{((2x-1)^2 + (2y-1)^2 + (2z-1.75)^2)}{0.5^2}} \text{ km/s.} \quad (15)$$

In computation, the velocity field v is rescaled by a factor $2/(\max_{0 \leq x, y, z \leq 1} v + \min_{0 \leq x, y, z \leq 1} v)$. We use a $159 \times 159 \times 159$ mesh. The source point is at $(x_0, y_0, z_0) = (0.5, 0.5, 0.5)$ km. Figure 10 shows the computed traveltimes and amplitudes at $z = 29/158$ km and $z = 109/158$ km.

We choose $\omega = 40\pi$ to construct the asymptotic Green's function. Figure 11 shows the comparisons between the constructed

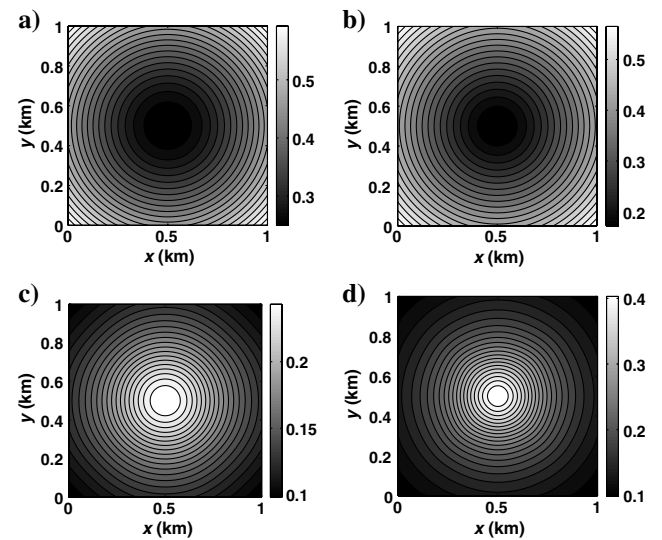


Figure 10. 3D example 2. (a) Traveltimes and (c) amplitudes at $z = 29/158$ km; (b) traveltimes and (d) amplitudes at $z = 109/158$ km.

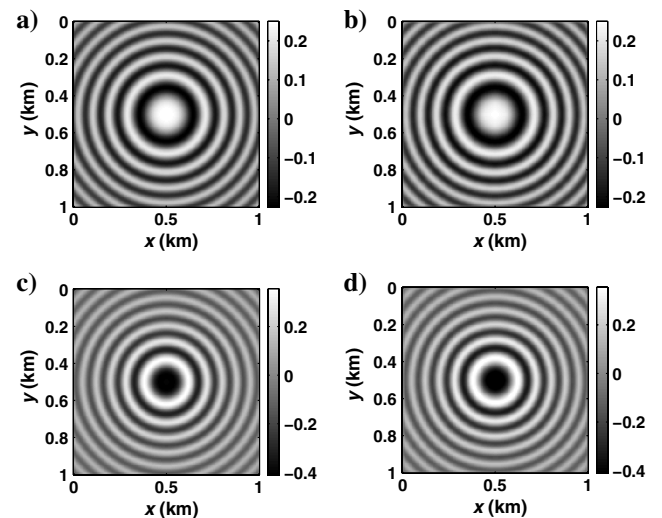


Figure 11. 3D example 2. Slice comparison of Green's functions with $\omega = 40\pi$. (a and b): Green's functions at $z = 29/158$ km; (c and d): Green's functions at $z = 109/158$ km. (a and c): Our method; (b and d): Helmholtz solver.

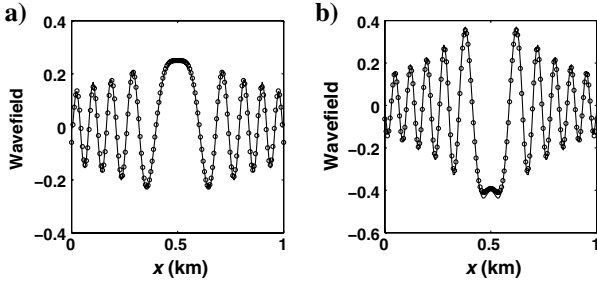


Figure 12. 3D example 2. Line comparison of Green's functions with $\omega = 40\pi$; (a) at $(y = 79/158, z = 29/158)$ km; (b) at $(y = 79/158, z = 109/158)$ km. Circle: our method; line: Helmholtz solver.

WKBJ Green's function and that obtained by the Helmholtz solver in Engquist and Ying (2011) at $z = 29/158$ km and $z = 109/158$ km. In Figure 12, we compare slices of the Green function at $(y = 79/158, z = 29/158)$ km and $(y = 79/158, z = 109/158)$ km, and this comparison indicates that the constructed asymptotic Green's function is accurate.

CONCLUSIONS

Based on the factored eikonal equation, we apply the factorization technique to compute the amplitude as well. To do that, we decompose the amplitude into two multiplicative factors, one of which is known analytically corresponding to a constant velocity field, capturing the source singularity of the amplitude. Then we apply the third-order WENO-based Lax-Friedrichs sweeping method to solve the factored equations for the underlying functions numerically. The advantage of decomposing the amplitude into two multiplicative factors is that because the known factor captures the source singularity, the other factor is smooth near the source. With computed traveltimes and amplitudes at our disposal, we construct asymptotic Green's functions in both 2D and 3D cases. Numerical examples are presented to demonstrate the performance of our method.

ACKNOWLEDGMENTS

Qian is partially supported by NSF 0810104, NSF 0830161, and NSF 1115363.

APPENDIX A

THIRD-ORDER WENO LAX-FRIEDRICHS SCHEME

We detail the Lax-Friedrichs scheme for the factored equations 7 and 9 on a rectangular mesh Ω^h with grid size h covering the domain Ω (Kao et al., 2004; Zhang et al., 2006; Luo and Qian, 2011). Let us consider equations in the following generic form,

$$H(x, y, z, u, u_x, u_y, u_z) = f(x, y, z). \quad (\text{A-1})$$

At grid point $(i, k, j) = (x_i, y_k, z_j)$ with neighbors,

$$N\{i, k, j\} = \{(x_{i-1}, y_k, z_j), (x_{i+1}, y_k, z_j), (x_i, y_k, z_{j-1}), (x_i, y_k, z_{j+1}), (x_i, y_{k+1}, z_j), (x_i, y_{k-1}, z_j)\},$$

we consider a Lax-Friedrichs Hamiltonian (Osher and Shu, 1991; Kao et al., 2004; Luo and Qian, 2011),

$$\begin{aligned} & H^{LF}(x_i, y_k, z_j, u_{i,k,j}, u_{N\{i,k,j\}}) \\ &= H\left(x_i, y_k, z_j, u_{i,k,j}, \frac{u_{i+1,k,j} - u_{i-1,k,j}}{2h}, \frac{u_{i,k+1,j} - u_{i,k-1,j}}{2h}, \frac{u_{i,k,j+1} - u_{i,k,j-1}}{2h}\right) \\ &\quad - \alpha_x \frac{u_{i+1,k,j} - 2u_{i,k,j} + u_{i-1,k,j}}{2h} - \alpha_y \frac{u_{i,k+1,j} - 2u_{i,k,j} + u_{i,k-1,j}}{2h} \\ &\quad - \alpha_z \frac{u_{i,k,j+1} - 2u_{i,k,j} + u_{i,k,j-1}}{2h}, \end{aligned} \quad (\text{A-2})$$

where α_x , α_y , and α_z are chosen such that for fixed (x_i, y_k, z_j) ,

$$\frac{\partial H^{LF}}{\partial u_{i,k,j}} \geq 0, \quad \frac{\partial H^{LF}}{\partial u_{N\{i,k,j\}}} \leq 0. \quad (\text{A-3})$$

For example, we can choose,

$$\begin{aligned} \alpha_x &= \max_{m \leq u \leq M, A \leq p \leq B, C \leq q \leq D, E \leq r \leq F} \left\{ \frac{1}{2} |H_1(x, y, z, u, p, q, r)| + \left| \frac{\partial H}{\partial u}(x, y, z, u, p, q, r) \right| \right\}, \\ \alpha_y &= \max_{m \leq u \leq M, A \leq p \leq B, C \leq q \leq D, E \leq r \leq F} \left\{ \frac{1}{2} |H_2(x, y, z, u, p, q, r)| + \left| \frac{\partial H}{\partial u}(x, y, z, u, p, q, r) \right| \right\}, \\ \alpha_z &= \max_{m \leq u \leq M, A \leq p \leq B, C \leq q \leq D, E \leq r \leq F} \left\{ \frac{1}{2} |H_3(x, y, z, u, p, q, r)| + \left| \frac{\partial H}{\partial u}(x, y, z, u, p, q, r) \right| \right\}, \end{aligned} \quad (\text{A-4})$$

where H_1 , H_2 , and H_3 denote the derivatives of H with respect to the first, second, and third gradient component, respectively. The flux H^{LF} is monotone for $m \leq u_{i,k,j} \leq M$, $A \leq p \leq B$, $C \leq q \leq D$ and $E \leq r \leq F$ with $p = (u_{i+1,k,j} - u_{i-1,k,j})/2h$, $q = (u_{i,k+1,j} - u_{i,k-1,j})/2h$ and $r = (u_{i,k,j+1} - u_{i,k,j-1})/2h$. Then we have a first-order Lax-Friedrichs scheme,

$$\begin{aligned} u_{i,k,j}^{new} &= \left(\frac{1}{\alpha_x/h + \alpha_y/h + \alpha_z/h} \right) \\ &\quad \times \left[f_{i,k,j} - H\left(x_i, y_k, z_j, u_{i,k,j}^{old}, \frac{u_{i+1,k,j} - u_{i-1,k,j}}{2h}, \frac{u_{i,k+1,j} - u_{i,k-1,j}}{2h}, \frac{u_{i,k,j+1} - u_{i,k,j-1}}{2h}\right) \right. \\ &\quad \left. + \alpha_x \frac{u_{i+1,k,j} + u_{i-1,k,j}}{2h} + \alpha_y \frac{u_{i,k+1,j} + u_{i,k-1,j}}{2h} + \alpha_z \frac{u_{i,k,j+1} + u_{i,k,j-1}}{2h} \right]. \end{aligned} \quad (\text{A-5})$$

As in Zhang et al. (2006) and Luo and Qian (2011), we replace $u_{i-1,k,j}$, $u_{i+1,k,j}$, $u_{i,k+1,j}$, $u_{i,k-1,j}$, $u_{i,k,j-1}$ and $u_{i,k,j+1}$ with,

$$\begin{aligned} u_{i-1,k,j} &= u_{i,k,j} - h(u_x)_{i,k,j}^-, \quad u_{i+1,k,j} = u_{i,k,j} + h(u_x)_{i,k,j}^+; \\ u_{i,k-1,j} &= u_{i,k,j} - h(u_y)_{i,k,j}^-, \quad u_{i,k+1,j} = u_{i,k,j} + h(u_y)_{i,k,j}^+; \\ u_{i,k,j-1} &= u_{i,k,j} - h(u_z)_{i,k,j}^-, \quad u_{i,k,j+1} = u_{i,k,j} + h(u_z)_{i,k,j}^+. \end{aligned} \quad (\text{A-6})$$

$(u_x)_{i,k,j}^-$ and $(u_x)_{i,k,j}^+$ are third-order WENO approximations of u_x , $(u_y)_{i,k,j}^-$ and $(u_y)_{i,k,j}^+$ are third-order WENO approximations of u_y , and $(u_z)_{i,k,j}^-$ and $(u_z)_{i,k,j}^+$ are third-order WENO approximations of u_z (see Osher and Shu, 1991; Liu et al., 1994; Jiang and Shu, 1996; and Jiang and Peng, 2000). For example,

$$\begin{aligned} (u_x)_{i,k,j}^- &= (1 - \omega_-) \left(\frac{u_{i+1,k,j} - u_{i-1,k,j}}{2h} \right) \\ &\quad + \omega_- \left(\frac{3u_{i,k,j} - 4u_{i-1,k,j} + u_{i-2,k,j}}{2h} \right) \end{aligned} \quad (\text{A-7})$$

with

$$\omega_- = \frac{1}{1 + 2\gamma_-^2}, \gamma_- = \frac{\epsilon + (u_{i,k,j} - 2u_{i-1,k,j} + u_{i-2,k,j})^2}{\epsilon + (u_{i+1,k,j} - 2u_{i,k,j} + u_{i-1,k,j})^2}, \quad (\text{A-8})$$

and

$$(u_x)_{i,k,j}^+ = (1 - \omega_+) \left(\frac{u_{i+1,k,j} - u_{i-1,k,j}}{2h} \right) + \omega_+ \left(\frac{-3u_{i,k,j} + 4u_{i+1,k,j} - u_{i+2,k,j}}{2h} \right) \quad (\text{A-9})$$

with

$$\omega_+ = \frac{1}{1 + 2\gamma_+^2}, \gamma_+ = \frac{\epsilon + (u_{i,k,j} - 2u_{i+1,k,j} + u_{i+2,k,j})^2}{\epsilon + (u_{i+1,k,j} - 2u_{i,k,j} + u_{i-1,k,j})^2}. \quad (\text{A-10})$$

Similarly, we can define third-order WENO approximations for $(u_y)_{i,k,j}^-, (u_y)_{i,k,j}^+, (u_z)_{i,k,j}^-$ and $(u_z)_{i,k,j}^+$. The term ϵ is a small positive number to avoid division by zero.

Then, we have a Lax-Friedrichs scheme based on the third-order WENO approximations (Zhang et al., 2006; Luo and Qian, 2011),

$$u_{i,k,j}^{\text{new}} = \left(\frac{1}{\alpha_x/h + \alpha_y/h + \alpha_z/h} \right) \times \left[f_{i,k,j} - H \left(x_i, y_k, z_j, u_{i,k,j}^{\text{old}}, \frac{(u_x)_{i,k,j}^- + (u_x)_{i,k,j}^+}{2}, \frac{(u_y)_{i,k,j}^- + (u_y)_{i,k,j}^+}{2}, \frac{(u_z)_{i,k,j}^- + (u_z)_{i,k,j}^+}{2} \right) + \alpha_x \frac{2u_{i,k,j}^{\text{old}} + h((u_x)_{i,k,j}^+ - (u_x)_{i,k,j}^-)}{2h} + \alpha_y \frac{2u_{i,k,j}^{\text{old}} + h((u_y)_{i,k,j}^+ - (u_y)_{i,k,j}^-)}{2h} + \alpha_z \frac{2u_{i,k,j}^{\text{old}} + h((u_z)_{i,k,j}^+ - (u_z)_{i,k,j}^-)}{2h} \right]. \quad (\text{A-11})$$

Here $u_{i,k,j}^{\text{new}}$ denotes the to-be-updated numerical solution for u at the grid point (i, k, j) and $u_{i,k,j}^{\text{old}}$ denotes the current old value for u at the same point.

REFERENCES

- Aldridge, D. F., 1994, Short note: Linearization of the eikonal equation: *Geophysics*, **59**, 1631–1632, doi: [10.1190/1.1443552](https://doi.org/10.1190/1.1443552).
- Alkhalifah, T., 2002, Traveltime computation with the linearized eikonal equation for anisotropic media: *Geophysical Prospecting*, **50**, 373–382, doi: [10.1046/j.1365-2478.2002.00322.x](https://doi.org/10.1046/j.1365-2478.2002.00322.x).
- Alkhalifah, T., and S. Fomel, 2010, An eikonal-based formulation for traveltime perturbation with respect to the source location: *Geophysics*, **75**, no. 6, T175–T183, doi: [10.1190/1.3490390](https://doi.org/10.1190/1.3490390).
- Babich, V. M., and V. S. Buldyrev, 2009: Asymptotic methods in short wave diffraction problems: Alpha Science International Ltd.
- Benamou, J. D., S. Luo, and H.-K. Zhao, 2010, A compact upwind second order scheme for the eikonal equation: *Journal of Computational Mathematics*, **28**, no. 4, 489–516, doi: [10.4208/jcm.1003-m0014](https://doi.org/10.4208/jcm.1003-m0014).
- Berenger, J.-P., 1994, A perfectly matched layer for the absorption of electromagnetic waves: *Journal of Computational Physics*, **114**, 185–200, doi: [10.1006/jcph.1994.1159](https://doi.org/10.1006/jcph.1994.1159).
- Bevc, D., 1997, Imaging complex structures with semirecursive Kirchhoff migration: *Geophysics*, **62**, 577–588, doi: [10.1190/1.1444167](https://doi.org/10.1190/1.1444167).
- Cerveny, V., I. A. Molotkov, and I. Psencik, 1977, Ray method in seismology: Univerzita Karlova Press.
- Crandall, M. G., and P.-L. Lions, 1983, Viscosity solutions of hamilton-jacobi equations: *Transactions of American Mathematical Society*, **277**, no. 1, 1–42.
- Engquist, B., O. Runborg, and A.-K. Tomberg, 2002, High frequency wave propagation by the segment projection method: *Journal of Computational Physics*, **178**, 373–390, doi: [10.1006/jcph.2002.7033](https://doi.org/10.1006/jcph.2002.7033).
- Engquist, B., and L. Ying, 2011, Sweeping preconditioner for the Helmholtz equation: Moving perfectly matched layers: *Multiscale Modeling and Simulation*, **9**, no. 2, 686–710, doi: [10.1137/100804644](https://doi.org/10.1137/100804644).
- Erlangga, Y. A., C. W. Oosterlee, and C. Vuik, 2006, A novel multigrid-based preconditioner for the heterogeneous Helmholtz equation: *SIAM Journal on Scientific Computing*, **27**, no. 4, 1471–1492, doi: [10.1137/040615195](https://doi.org/10.1137/040615195).
- Fomel, S., S. Luo, and H.-K. Zhao, 2009, Fast sweeping method for the factored eikonal equation: *Journal of Computational Physics*, **228**, 6440–6455, doi: [10.1016/j.jcp.2009.05.029](https://doi.org/10.1016/j.jcp.2009.05.029).
- Fomel, S., and J. Sethian, 2002, Fast phase space computation of multiple traveltimes: *Proceedings of the National Academy of Sciences*, **99**, 7329–7334.
- Franklin, J., and J. M. Harris, 2001, A high-order fast marching scheme for the linearized eikonal equation: *Journal of Computational Acoustics*, **9**, 1095–1109.
- Geoltrain, S., and J. Brac, 1993, Can we image complex structures with first-arrival traveltime: *Geophysics*, **58**, 564–575, doi: [10.1190/1.1443439](https://doi.org/10.1190/1.1443439).
- Gray, S., and W. May, 1994, Kirchhoff migration using eikonal equation traveltimes: *Geophysics*, **59**, 810–817, doi: [10.1190/1.1443639](https://doi.org/10.1190/1.1443639).
- Jiang, G. S., and D. Peng, 2000, Weighted ENO schemes for Hamilton-Jacobi equations: *SIAM Journal on Scientific Computing*, **21**, no. 6, 2126–2143, doi: [10.1137/S106482759732455X](https://doi.org/10.1137/S106482759732455X).
- Jiang, G. S., and C. W. Shu, 1996, Efficient implementation of weighted ENO schemes: *Journal of Computational Physics*, **126**, 202–228, doi: [10.1006/jcph.1996.0130](https://doi.org/10.1006/jcph.1996.0130).
- Jo, C.-H., C. Shin, and J. H. Suh, 1996, An optimal 9-point, finite-difference, frequency-space, 2-D scalar wave extrapolator: *Geophysics*, **61**, 529–537, doi: [10.1190/1.1443979](https://doi.org/10.1190/1.1443979).
- Kao, C. Y., S. Osher, and J. Qian, 2004, Lax-friedrichs sweeping schemes for static hamilton-jacobi equations: *Journal of Computational Physics*, **196**, 367–391, doi: [10.1016/j.jcp.2003.11.007](https://doi.org/10.1016/j.jcp.2003.11.007).
- Kim, S., and R. Cook, 1999, 3-D traveltime computation using second-order ENO scheme: *Geophysics*, **64**, 1867–1876, doi: [10.1190/1.1444693](https://doi.org/10.1190/1.1444693).
- Leung, S., and J. Qian, 2006, An adjoint state method for three-dimensional transmission traveltime tomography using first-arrivals: *Communications in Mathematical Sciences*, **4**, no. 1, 249–266.
- Leung, S., J. Qian, and R. Burridge, 2007, Eulerian Gaussian beams for high-frequency wave propagation: *Geophysics*, **72**, no. 5, SM61–SM76, doi: [10.1190/1.2752136](https://doi.org/10.1190/1.2752136).
- Leung, S., J. Qian, and S. Osher, 2004, A level set method for three dimensional paraxial geometrical optics with multiple sources: *Communications in Mathematical Sciences*, **2**, no. 4, 657–686.
- Lions, P.-L., 1982, Generalized solutions of Hamilton-Jacobi equations: Pitman.
- Liu, X. D., S. Osher, and T. Chan, 1994, Weighted essentially nonoscillatory schemes: *Journal of Computational Physics*, **115**, 200–212, doi: [10.1006/jcph.1994.1187](https://doi.org/10.1006/jcph.1994.1187).
- Luo, S., and J. Qian, 2011, Factored singularities and high-order Lax-Friedrichs sweeping schemes for point-source traveltimes and amplitudes: *Journal of Computational Physics*, **230**, 4742–4755, doi: [10.1016/j.jcp.2011.02.043](https://doi.org/10.1016/j.jcp.2011.02.043).
- Meng, Z., and N. Bleistein, 1997, Wavefront construction ray tracing in tetrahedral models-application to 3-D traveltime and ray path computations: 67th Annual International Meeting, SEG, Expanded Abstracts, 1734–1737.
- Nichols, D., 1994, Imaging complex structures using band limited Green's functions: Ph.D. thesis, Stanford University.
- Osher, S., L.-T. Cheng, M. Kang, H. Shim, and Y. Tsai, 2002, Geometrical optics in a phase space based level set and Eulerian framework: *Journal of Computational Physics*, **179**, 622–648, doi: [10.1006/jcph.2002.7080](https://doi.org/10.1006/jcph.2002.7080).
- Osher, S., and C.-W. Shu, 1991, High-order essentially nonoscillatory schemes for Hamilton-Jacobi equations: *SIAM Journal on Numerical Analysis*, **28**, 907–922, doi: [10.1137/0728049](https://doi.org/10.1137/0728049).
- Pereyra, V., W. H. Lee, and H. B. Keller, 1980, Solving two-point seismic-ray tracing problems in a heterogeneous medium: *Bulletin of the Seismological Society of America*, **70**, 79–99.
- Pica, A., 1997, Fast and accurate finite-difference solutions of the 3d eikonal equation parametrized in celerity: 67th Annual International Meeting, SEG, Expanded Abstracts, 1774–1777.
- Podvin, P., and I. Lecomte, 1991, Finite difference computation of traveltimes in very contrasted velocity models: A massively parallel approach and its associated tools: *Geophysical Journal International*, **105**, 271–284, doi: [10.1111/gji.1991.105.issue-1](https://doi.org/10.1111/gji.1991.105.issue-1).
- Qian, J., L.-T. Cheng, and S. Osher, 2003, A level set based Eulerian approach for anisotropic wave propagations: *Wave Motion*, **37**, 365–379, doi: [10.1016/S0165-2125\(02\)00101-4](https://doi.org/10.1016/S0165-2125(02)00101-4).
- Qian, J., and S. Leung, 2004, A level set method for paraxial multivalued traveltimes: *Journal of Computational Physics*, **197**, 711–736, doi: [10.1016/j.jcp.2003.12.017](https://doi.org/10.1016/j.jcp.2003.12.017).

- Qian, J., and S. Leung, 2006, A local level set method for paraxial multivalued geometric optics: *SIAM Journal on Scientific Computing*, **28**, no. 1, 206–223, doi: [10.1137/030601673](https://doi.org/10.1137/030601673).
- Qian, J., and W. W. Symes, 2002a, An adaptive finite-difference method for traveltimes and amplitudes: *Geophysics*, **67**, 167–176, doi: [10.1190/1.1451472](https://doi.org/10.1190/1.1451472).
- Qian, J., and W. W. Symes, 2002b, Finite-difference quasi-P traveltimes for anisotropic media: *Geophysics*, **67**, 147–155, doi: [10.1190/1.1451438](https://doi.org/10.1190/1.1451438).
- Qian, J., Y.-T. Zhang, and H.-K. Zhao, 2007a, A fast sweeping methods for static convex Hamilton-Jacobi equations: *Journal for Scientific Computing*, **31**, 1–2, 237–271, doi: [10.1007/s10915-006-9124-6](https://doi.org/10.1007/s10915-006-9124-6).
- Qian, J., Y.-T. Zhang, and H.-K. Zhao, 2007b, Fast sweeping methods for eikonal equations on triangulated meshes: *SIAM Journal on Numerical Analysis*, **45**, 83–107, doi: [10.1137/050627083](https://doi.org/10.1137/050627083).
- Qin, F., Y. Luo, K. B. Olsen, W. Cai, and G. T. Schuster, 1992, Finite difference solution of the eikonal equation along expanding wavefronts: *Geophysics*, **57**, 478–487, doi: [10.1190/1.1443263](https://doi.org/10.1190/1.1443263).
- Rawlinson, R., and M. Sambridge, 2004, Wave front evolution in strongly heterogeneous layered media using the fast marching method: *Geophysical Journal International*, **156**, 631–647, doi: [10.1111/gji.2004.156.issue-3](https://doi.org/10.1111/gji.2004.156.issue-3).
- Sava, P., and S. Fomel, 2001, 3-d traveltimes computation using Huygens wavefront tracing: *Geophysics*, **66**, 883–889, doi: [10.1190/1.1444977](https://doi.org/10.1190/1.1444977).
- Schneider, W. A. J., 1995, Robust and efficient upwind finite-difference traveltimes calculations in three dimensions: *Geophysics*, **60**, 1108–1117, doi: [10.1190/1.1443839](https://doi.org/10.1190/1.1443839).
- Schneider, W. A. J., K. Ranzinger, A. Balch, and C. Kruse, 1992, A dynamic programming approach to first arrival traveltimes computation in media with arbitrarily distributed velocities: *Geophysics*, **57**, 39–50, doi: [10.1190/1.1443187](https://doi.org/10.1190/1.1443187).
- Serna, S., and J. Qian, 2010, A stopping criterion for higher-order sweeping schemes for static Hamilton-Jacobi equations: *Journal of Computational Mathematics*, **28**, no. 4, 552–568.
- Sethian, J. A., and A. M. Popovici, 1999, 3-D traveltimes computation using the fast marching method: *Geophysics*, **64**, 516–523, doi: [10.1190/1.1444558](https://doi.org/10.1190/1.1444558).
- Symes, W. W., and J. Qian, 2003, A slowness matching Eulerian method for multivalued solutions of eikonal equations: *Journal for Scientific Computing*, **19**, no. 1–3, 501–526, doi: [10.1023/A:1025380731197](https://doi.org/10.1023/A:1025380731197).
- Taillandier, C., M. Noble, and H. Calandra, 2008, A massively parallel 3-D refraction traveltimes tomography algorithm: 70th Annual Conference and Exhibition, EAGE, Extended Abstracts, 1–5.
- Taillandier, C., M. Noble, H. Chauris, and H. Calandra, 2009, First-arrival traveltimes tomography based on the adjoint-state method: *Geophysics*, **74**, WCB1–WCB10, doi: [10.1190/1.3250266](https://doi.org/10.1190/1.3250266).
- Taillandier, C., M. Noble, H. Chauris, P. Podvin, H. Calandra, and J. Guilbot, 2007, Refraction traveltimes tomography based on adjoint state techniques: 69th Annual Conference and Exhibition, EAGE, Extended Abstracts, 1–5.
- Tryggvason, A., and B. Bergman, 2006, A traveltimes reciprocity discrepancy in the Podvin & Lecomte *time3D* finite difference algorithm: *Geophysical Journal International*, **165**, 432–435, doi: [10.1111/gji.2006.165.issue-2](https://doi.org/10.1111/gji.2006.165.issue-2).
- Tsai, Y., L.-T. Cheng, S. Osher, and H.-K. Zhao, 2003, Fast sweeping algorithms for a class of Hamilton-Jacobi equations: *SIAM Journal on Numerical Analysis*, **41**, 673–694, doi: [10.1137/S0036142901396533](https://doi.org/10.1137/S0036142901396533).
- van Trier, J., and W. W. Symes, 1991, Upwind finite-difference calculation of traveltimes: *Geophysics*, **56**, 812–821, doi: [10.1190/1.1443099](https://doi.org/10.1190/1.1443099).
- Vidale, J. E., 1990, Finite-difference calculation of traveltimes in three dimensions: *Geophysics*, **55**, 521–526, doi: [10.1190/1.1442863](https://doi.org/10.1190/1.1442863).
- Vinje, V., E. Iversen, K. Astebol, and H. Gjoystdal, 1996, Estimation of multivalued arrivals in 3D models using wavefront construction — Part I: *Geophysical Prospecting*, **44**, 819–842, doi: [10.1111/gpr.1996.44.issue-5](https://doi.org/10.1111/gpr.1996.44.issue-5).
- Vinje, V., E. Iversen, and H. Gjoystdal, 1993, Traveltimes and amplitude estimation using wavefront construction: *Geophysics*, **58**, 1157–1166, doi: [10.1190/1.1443499](https://doi.org/10.1190/1.1443499).
- Zhang, L., J. W. Rector, and G. M. Hoversten, 2005, Eikonal solver in the celerity domain: *Geophysical Journal International*, **162**, 1–8, doi: [10.1111/gji.2005.162.issue-1](https://doi.org/10.1111/gji.2005.162.issue-1).
- Zhang, Y.-T., H.-K. Zhao, and J. Qian, 2006, High order fast sweeping methods for static Hamilton-Jacobi equations: *Journal for Scientific Computing*, **29**, no. 1, 25–56, doi: [10.1007/s10915-005-9014-3](https://doi.org/10.1007/s10915-005-9014-3).
- Zhao, H.-K., 2005, A fast sweeping method for eikonal equations: *Mathematics of Computation*, **74**, 603–628, doi: [10.1090/S0025-5718-04-01678-3](https://doi.org/10.1090/S0025-5718-04-01678-3).